Article:
Godinho Cassol, H.L., De Oliveira E Cruz De Aragão, L.E., Moraes, E.C. et al. (2021) Quad-pol advanced land observing satellite/phased array L-band synthetic aperture radar-2 (ALOS/PALSAR-2) data for modelling secondary forest above-ground biomass in the central Brazilian Amazon. International Journal of Remote Sensing, 42 (13). pp. 4985-5009. ISSN: 0143-1161

https://doi.org/10.1080/01431161.2021.1903615

This is an Accepted Manuscript of an article published by Taylor & Francis in International Journal of Remote Sensing on 8th April 2021, available online:
http://www.tandfonline.com/10.1080/01431161.2021.1903615

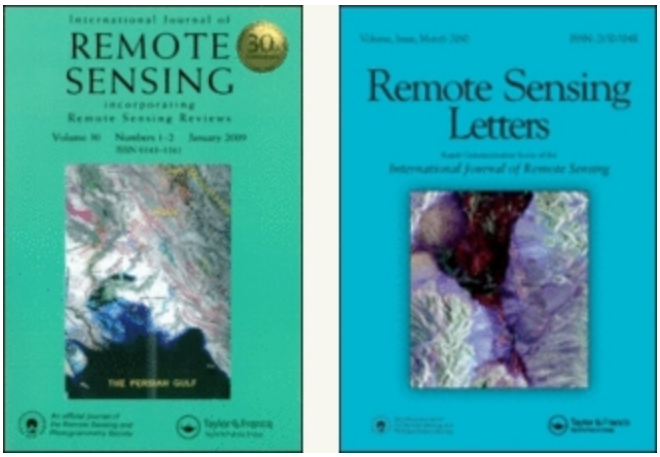

Quad-pol ALOS/PALSAR-2 data for modelling secondary forest above-ground biomass in the central Brazilian Amazon

Journal:	*International Journal of Remote Sensing*
Manuscript ID	TRES-PAP-2020-1127
Manuscript Type:	IJRS Research Paper
Date Submitted by the Author:	15-Sep-2020
Complete List of Authors:	Cassol, Henrique Luis; National Institute for Space Research, Remote Sensing Division Aragão, Luiz Eduardo; National Institute for Space Research, Remote Sensing Division Caria Moraes, Elisabete; National Institute for Space Research, Remote Sensing Division Carreiras , João ; The University of Sheffield, National Centre for Earth Observation (NCEO) Shimabukuro, Yosio; National Institute for Space Research, Remote Sensing Division
Keywords:	Polarimetric SAR, radar backscatter, Decomposition, SAR PROCESSING
Keywords (user defined):	

Quad-pol ALOS/PALSAR-2 data for modelling secondary forest above-ground biomass in the central Brazilian Amazon

Henrique Luis Godinho Cassol[a*], Luiz Eduardo de Oliveira e Cruz de Aragão[a], Elisabete Caria Moraes[a], João Manuel de Brito Carreiras[b] and Yosio Edemir Shimabukuro[a]

[a] *Remote Sensing Division, National Institute for Space Research (INPE), São José dos Campos, Brazil;*

[b]*National Centre for Earth Observation (NCEO), University of Sheffield, UK;*

* National Institute for Space Research (INPE), Remote Sensing Division, Av. dos Astronautas 1758, Jd. Granja, São José dos Campos, São Paulo, Brazil. Henrique.cassol@inpe.br

Quad-pol ALOS/PALSAR-2 data for modelling secondary forest above-ground biomass in the central Brazilian Amazon

Secondary forests (SFs) are one of the major carbon sinks in the Neotropics due to the rapid carbon assimilation in their above-ground biomass (AGB). However, the accurate contribution of SFs to the carbon cycle is a great challenge because of the uncertainty in AGB estimates. In this context, the main objective of this study is to explore full polarimetric ALOS/PALSAR-2 data to model SFs AGB in the Central Amazon. We carried out the forest inventory in 2014, measuring 23 field plots. Supplementary land-use classification history was used to create 120 additional independent sample plots by adjusting growth curves using SFs age and previous land-use intensity from field plots. Multiple Linear Regression (MLR) analysis was performed to select the best model by corrected weighted Akaike Information Criterion (AICw) and validated by the leave-one-out bootstrapping method. The best-fitted model has six parameters and explained 65% of the above-ground biomass variability. The prediction error was of RMSEP = 8.8 ± 3 Mg ha^{-1} (8.75%). The main polarimetric attributes in the model were those directly related to multiple scattering mechanisms as the Shannon Entropy and the volumetric mechanism of Bhattacharya decomposition, and those related to increasing in double-bounce as the co-polarization ratio (VV/HH) resulted from soil-trunk interactions. Including past-use use in the model, as the frequency of clear cuts and the number of years of active land-use before abandonment, the variability explained by the MLR increased by 10%. The uncertainty report showed that ground truth AGB estimation (inventory, allometry, and plot expansion factors) might add more errors than SAR inversion models.

Keywords: Amazon Forest; Polarimetry; Synthetic Aperture Radar; Scattering Decomposition; Second Growth

Subject classification codes: include these here if the journal requires them

1. Introduction

The areas undergoing regeneration are partially counterbalancing the carbon emissions from deforestation, forest degradation, forest fires, and other sources from land-use change processes, accumulating carbon in their above-ground biomass (AGB). In the

Brazilian Amazon, secondary forests (SFs) have the potential to accumulate over 6 Pg C in 40 years (Chazon et al. 2016). It accounts for one-third of Brazil's total annual CO_2 emissions during the 2000-2009 period (Houghton et al. 2012). So, carbon uptake by SFs is a crucial element in the global carbon budget, which requires the need to accurately estimate their AGB stocks and growth rates (Aragão et al. 2014). The rate of forest regeneration depends on several factors to which the area was subjected before abandonment, such as severity, the proximity of forest matrix, duration of the previous land-use, and frequency of clearances (Chazdon, 2014; Wandelli and Fearnside, 2015). For instance, an intensive land-use before regeneration reduces the rate of growth and can compromise the resilience of the tropical ecosystem by arresting forest succession following disturbances or even leading to alternative stable states (Scheffer et al. 2012). The historical use information, however, is generally not taken into account when retrieving forest AGB using remote sensing techniques.

When the microwave pulses reach the canopy layer, they suffer multiple scatterings in all directions, and the recorded backscatter by the sensor is a result of the structure and geometric properties of the forest targets at the same wavelength. Thus, the higher the biomass density, the greater the backscatter recorded by the sensor (van der Sanden, 1997). With the upcoming of polarimetric SAR systems (operating in four polarizations), other levels of relationship with the forest targets are achieved, allowing to decompose the recorded wave in three or more elementary scattering mechanisms that depend only on the target's properties, such as volume, structure, and forest characteristics (Santos et al. 2009). Such polarimetric decompositions are useful to characterize these complex targets, increasing, above all, the accuracy of biomass estimates (Bispo et al. 2014; Treuhaft et al. 2017; Lee and Pottier, 2009; Sinha et al. 2015; Cassol et al. 2018a). Some of these features, resulting from the decomposition

process, were never tested to predict forest AGB or were applied only to land-use classification in specific areas (Singh, Yamaguchi, and Park, 2013; Zhang et al. 2008; Bharadwaj et al. 2015; Bhattacharya et al. 2015; Neumann, Ferro-Famil, and Pottier, 2009).

Historically, modelling AGB in the Brazilian Amazon has been carried out through the information obtained by Radar (Radio-Detection and Range) data, due to two main reasons: they operate in all-weather condition, and they have higher sensitivity of the signal to AGB when compared with optical observations (Bispo et al. 2014; Treuhaft et al. 2017). The Advanced Land Observing Satellite / Phased Array L-band Synthetic Aperture Radar-2 (ALOS/PALSAR-2), which operates in microwaves (L-band, 23.5 cm), capture images during day and night and is insensitive to cloud cover (Lee and Pottier, 2009).

The goal of this work is to evaluate the use of full polarimetric (Quad-pol) ALOS/PALSAR-2 data to retrieve AGB of SFs at the Manaus study site, Amazonas State in the Central Amazonia, using multiple linear regression analysis. We explored 125 polarimetric attributes from the ALOS/PALSAR-2, including some unusual as off-diagonal terms of the covariance **[C]** and coherency **[T]** matrices for modelling SFs biomass. Previously, we increased data sampling by creating 120 additional sample plots based on growth models of previous land-use classification (Carreiras et al. 2014) and field inventory data.

2. Materials and Methods

The study area comprises SFs formed on both sides of BR-174 highway, 70 km north of the city of Manaus. This area has 5,042 km² (2º33'11"S, 60º5'7'W) and includes

protected areas and long-term ecological experiments, such as the Biological Dynamics of Forest Fragments Project (BDFFP), started in 1979 (Figure 1a) (Laurance et al. 2018).

The process of deforestation in the region began with the construction of the BR-174 highway in the mid-1970s, where significant forest areas were suppressed around the highway that connects Manaus, Amazonas State, to Boa Vista, Roraima State. However, due to low agricultural capability and the extinction of government subsidies, many of these areas were abandoned after 1984 (Feldpausch et al. 2005). As a result of these idle areas, SFs have over 16 years of age in 50% of the REGROWTH-BR project area (Carreiras et al. 2014), as depicted in Figure 1b.

The climate is classified as Am (Köppen), with an annual mean temperature of 26.7 °C and an annual average rainfall of 2200 mm. The dry season occurs from July to September with rainfall below 100 mm in this period. The vegetation is considered as Terra Firme rainforest, with canopy height between 25 and 35 m, with some emergent trees reaching 40 m in favourable sites (Lima et al. 2007). The methodological flowchart is shown in Figure 2. The described steps are summarized in the following sections and subsections.

2.1. Sampling design

The sampling strategy was carried out in three main stages with the aiming of expanding the data set, as follows:

- forest inventory data (23 plots measured in this study);
- modelling SFs growth (additional 76 plots with auxiliary forest inventory plots from the literature), and
- creation of 120 samples based on Landsat classification time series and SFs growth curves (Figure 2).

The detailed description of each of these processes is shown in the following sections. Random sampling was chosen to guarantee independence among samples allowing to compute uncertainty and errors independently.

2.2. Landsat time series classification

This area was part of the international project REGROWTH-BR, completed in 2015, and carried out in partnership between the Tropical Research Institute IICT/Lisbon, School of Agriculture/ University of Lisbon ISA/Lisbon, and the National Institute for Space Research (INPE). As a part of the project, Landsat time series classification was performed annually from 1984 to 2010 at the study site using the machine learning algorithms (Carreiras et al. 2014). This classification allowed the extraction of several secondary forest metrics, including forest age (years since deforestation event), the frequency of clear cuts (number of clear cuts), and period of active land-use - PALU (years of agriculture or livestock practices before being abandoned and forest regrowth) (Figure 1b). The authors updated the classification for data image acquisition (2016).

2.3. Inventory data

The forest inventory was carried out in August 2014, measuring 23 field plots (white triangles in Fig 1a). Field plots were randomly selected in SFs, with ages varying from 12 to 34 years, according to land-use history obtained by the REGROWTH-BR project (Carreiras et al. 2014, Figure 1b). These plots were subsequently grouped into two intensity class of use prior abandonment (see section 2.3.2) to expand the sample size for the growth models (Figure 2).

The method consisted of nested transects with different sizes, ranging from 10 x 100 m for the measurement of small tree individuals with diameters at breast height DBH ≥ 5 cm, up to 60 x 100 m to measure large-trees (DBH ≥ 20 cm). The arboreal

individuals were identified by species and botanical family by an experienced parataxonomist and had its scientific names checked in the site: www.theplantlist.org (Cassol et al. 2018b). Also, we computed some phytosociological parameters, such as basal area (G), the number of species (S), and the number of individuals per hectare (N).

2.3.1. Above-ground biomass

The equation to estimate above-ground biomass (AGB) in living trees at the Manaus study site was given in Brown, Gillespie, and Lugo (1989):

$$AGB_{\text{live}} = e^{(-2.41 + 0.952 \ln (DBH^2 h \rho)} \quad (1)$$

where AGB_{live} is the above-ground dry mass (kg), DBH is the diameter at breast height (cm), ρ is the wood density (g cm^{-3}), h is the total tree height (m), obtained by hypsometric equations adjusted by ecological species group (Cassol et al. 2018b). The AGB from standing dead trees and palm trees were estimated by different methodologies, as described in Cassol et al. (2018b). The total AGB was extrapolated to the hectare by the sum of the individual tree weights in each plot (Mg ha^{-1}).

2.3.2. Classes of Intensity from the previous land-use

The land-use history was assessed for two purposes: (i) to model secondary forest growth as a function of past land-use, as reported by Wandelli and Fearnside (2015) and (ii) to create an additional 120 independent sample plots for retrieving AGB using polarimetric ALOS/PALSAR-2 data. Intensity classes separated land-use before abandonment as (1) low intensity - one clear cut (deforestation event) and PALU ≤ 2 years; (2) high intensity - two or more clear cuts and PALU > 2 years (Figure 3).

Visually, we can see a clear separation of the structure and species distribution of the secondary forest's profiles regarding intensity class in Figure 3. In A and B there is a well-structured forest, well-distribution of individuals in all classes of diameter, and

less light reaching the understory. Note the higher incidence of vines and lianas, in C and D (Figure 3).

There are significant differences in phytosociological parameters measured in the field according to intensity classes based on the Kolmogorov-Smirnoff test (Figure 4, p-value<0.005). In general, when initial disturbances are small, and land-use has a short duration, the phytosociological parameters recover quickly. Low-intensity use areas have higher values of stand parameters, such as average diameter, mean tree height, basal area, number of species, and forest AGB (Figure 4).

The exception was the number of individuals per hectare (N), which has fewer individuals in low-intensity use areas. Secondary forest AGB was significantly higher in low-intensity areas than in high intensity used areas before abandonment (μ_1 = 188.4 Mg ha^{-1}, μ_2 = 178.3 Mg ha^{-1}, p-value<0.001, Figure 2). These differences in AGB accumulation and phytosociological parameters support the treatment of SF growth by intensity class.

2.3.3. Modelling tree growth

As the number of samples may be a limiting factor to retrieve forest AGB (Sinha et al. 2015), we model secondary forest growth by its age and intensity class to create new independently AGB samples from the classified Landsat time series Figure 2b (Carreiras et al. 2014). Furthermore, the purpose was to correct the values of AGB collected during the field inventory in 2014 for the satellite overpass date (2016).

Therefore, to improve the model fit, we collected other 76 secondary forest plots within the same study area describing the AGB, age, and intensity class, which were added to the analysis, totalizing 99 1-ha plots (Gehring, Denich, and Vlek, 2005; Prates-Clark, Lucas, and Santos, 2009; Steininger, 2000; Feldpausch et al. 2005; Lima et al.

2007; Silva, 2007).

The model used was a three parameters Chapman-Richards model adjusted by Nonlinear Mixed-Effects model (Pinheiro and Bates, 2000), where forest stand age was treated as a fixed factor and the intensity class as a random effect (Table 1). Low-intensity land-use accumulates more AGB in secondary forests up to 10 years (Figure 5a); the Mean Annual Increment (MAI) in low-intensity areas is almost twice the increment of high-intensity areas in the early years (Figure 5b). After 20 years of abandonment, SFs AGB presents similar growth curves and increment regardless of their past land-use.

2.3.4. Additional sampling

Appling specific growth curves from Figure 5a, a total of 120 samples of AGB in the study area (60 from intensity class IC = 1, and 60 from IC = 2) were created. The new independent secondary forest samples were randomly located in the classification of the Landsat times series, aged between 1 to 32 years, ranging from low to high-intensity use classes (Figure 1b). The sample size was the same as inventory plots (60 x 100 m). Finally, these 120 samples form the dataset for retrieving SFs AGB from ALOS/PALSAR-2.

2.4. ALOS/PALSAR-2 data processing

Two full-polarimetric scenes were acquired for the study area in CEOS SAR format, processing level 1.1. (Single Look Complex) in slant range high sensitive mode. The acquisition dates were 04 and 18 April 2016, obtained in the ascending orbit to the right of the antenna at 4:15 pm. The angle of incidence ranged from 33.8 to 36.5° to the dates of April 4 and April 18, respectively. According to the meteorological institute of Brazil

(INMET), rainfall prior to acquisition time was negligible.

The pre-processing steps were the following: multilook, filtering, extraction of attributes derived from covariance and coherence matrices, polarimetric decompositions, calibration, and geocoding (Figure 2). The multilook process is a resampling step towards the azimuth applied to produce images with regular dimensions, as well as to reduce the speckle effect (Lee and Pottier, 2009). The range and azimuth resampling factor were set at 1:2, resulting in a nominal spatial resolution of approximately 6.25 m. The speckle was reduced by the Refined Lee filter (11x11 pixels window size), which was considered optimal for our analysis (Cassol et al. 2018a). This filter size was a trade-off between the gain obtained by the indiscriminate increase of the filter size and the loss of relevant radiometric information caused by spatial smoothing (Lee and Pottier, 2009). The polarimetric decomposition involved the extraction of 125 polarimetric attributes from coherence **[T]** and covariance **[C]** matrices and used as predictors of multiple linear regressions models to retrieve AGB. The full-list description is given in Table A.1. (Appendix I).

The conversion of the digital numbers from the SLC image to the backscatter coefficient σ° (sigma nought, in dB) in the four polarizations (HV = VH) was performed by (2):

$$\sigma^0 = 10\, log_{10}(I^2 + Q^2) + CF \qquad (2)$$

where I is the in-phase and Q is the quadrature in the SLC data; CF is the absolute calibration factor and has the value of -83 dB (Shimada et al. 2009).

After calibration and extraction of polarimetric attributes, the Range-Doppler Terrain Correction performs image geocoding (Small and Schubert, 2008). This process executes the SAR orthorectification with the precise transformation of slant-range to

ground-range using a Digital Elevation Model (DEM) from SRTM (www.usgs.gov/srtm).

2.5. Partial Correlation and Feature Selection

To reduce data dimensionality, the "CFS filter" algorithm proposed by Hall (1999) applies a variable selection in the FSelector package (Romanski and Kotthoff, 2014) in the R Core Team (2017). According to the authors, the Correlation-based Feature Selection (CFS) is an algorithm that selects a subset of attributes based on correlation coefficients and the concept of information entropy (Hall, 1999). This step was critical to avoid catching similar information from polarimetric decompositions, such as distinct volumetric scattering mechanisms. The dataset was randomized into ten subsets by the leave-one-out cross-validation process resulting in the best polarimetric attributes subset. Attributes that appear in 90% of cases were used as selection criteria to model SFs AGB.

2.6. Multiple linear regression models (MLR)

In the multiple linear regression models, the AGB (Y) dependent variable is estimated by multiple independent variables (X) from the ALOS/PALSAR-2 images by a linear relationship between these variables (3):

$$Y_i = \beta_0 + \beta_1 X_{i,1} + \beta_2 X_{i,2} + \ldots + \beta_p X_{i,p} + \varepsilon_i \quad (3)$$

where Y_i is the AGB in the *i-th* observation in Mg ha^{-1}, β_0, β_1, β_2,…, β_p are the model parameters, $X_{i,1}$, $X_{i,2}$,…, $X_{i,p}$ are the p explanatory variables of the model in the *i-th* observation and the ε_i is the random error.

The analysis was performed using the exhaustive selection package of variables "glmulti" implemented in R through the ordinary least square's method (Calcagno and

Mazancourt, 2010). Model selection was performed by the AIC criterion, where the models with Δ AIC < 2 were chosen, and the best model was determined by the weights given to the set of explanatory variables in the model – Akaike weights (w_i) (Burnham and Anderson, 2002). According to the authors, w_i is the relative likelihood of the model, given the data. These are normalized to sum 1 and interpreted as probabilities. So, the ratio of Akaike weights w_i/w_j can be judged in favour of the best model against alternative model w_j. We also evaluated the best MLR model by the following criteria, defined by (Motulsky and Christopoulos, 2003): i) the significance of the estimate parameters, standard error (Sy), and Variance Inflation Factor (VIF) of the regression parameters; ii) the distribution of the standardized residuals to verify the absence of outliers; and iii) the Breusch-Pagan test for the homoscedasticity of the residuals.

2.7. Model validation

The validation of the regression models was evaluated by the coefficient of determination (R^2) between the values predicted by the regression and the values from the validation samples and by the distribution error of prediction, i.e., by Root Mean Square Error of the Prediction (RMSEP) (Motulsky and Christopoulos, 2003) (4):

$$RMSEP = \sqrt{bias^2 + \sigma_{bias}^2} \quad (4)$$

where bias is the difference between the observed and the expected value from MLR, using validation sample. The distribution of the prediction bias was analyzed by the t-test considering the null hypothesis of bias deviation equal to zero (without trend). The selection of the best MLR model, therefore, combines the highest w_i value and lowest RMSEP. The bootstrap method with 100 repetitions was performed iteratively to build the model and its confidence intervals, keeping 80% of samples for training and 20% of samples for validation (Figure 2).

2.8. Uncertainty Analysis

We also assessed the major uncertainties considering retrieving forest AGB in different stages of the estimation procedure. Understanding the source errors is critical to perform wall-to-wall mapping of forest AGB, which is challenging in heterogeneous complex tropical environments (Sinha et al. 2015). For the propagation of errors calculated here, we assumed that all errors were distributed independently, uncorrelated, and random. In order to make a comparison among scale and units, we reported the uncertainty through relative mean errors (%). The propagation error (δQ) was defined by (5) (Motulsky and Christopoulos, 2003):

$$\delta Q = \sqrt{(\delta a)^2 + (\delta b)^2 + (\delta c)^2 + \ldots + (\delta z)^2} \quad (5)$$

where δQ is the square root of the sum squares or the mean uncertainty, and δa, δb, …, δz are the specific uncertainties in percentage (%).

3. Results and Discussion

3.1. Performance of the Multiple Linear Models

Ten attributes were chosen as the best predictors of the SFs AGB using CFS feature selection. The selected attributes were those from the multiple scattering mechanisms from the canopy, such as the Bhattacharya and Yamaguchi volumetric scattering components, the Shannon Entropy (*SE*), and the cross-polarization ratio (*Rcp*). The attributes from the VV channel, whose responses are mostly related to the double-bounce scattering components such as co-polarization ratio (*Rpp*), which becomes more significant as the forest AGB increases (Figure 6).

The other attributes were related to the structure of the SFs, which, due to the orientation of the multiple scatters, changes the signal phase return and causes

depolarization between the polarimetric channels (Table 2). These attributes are the terms off-diagonal of the coherency matrix $\mathbf{[T]_{3x3}}$ and the phase magnitude of the first Touzi component (Φs_1) and showed lowest with SFs AGB ($\rho < 0.28$); the highest correlation with SFs AGB was the contribution volumetric scattering mechanism obtained from four-component model-based polarimetric decompositions, Bhattacharya and Yamaguchi (ρ = 0.77-0.78) (Figure A.1, Appendix). According to the authors (Yamaguchi et al. 2005; Bhattacharya et al. 2015), the four-component decomposition model, instead of three as originally proposed by Freeman and Durden (1998), added the helix scattering term in non-reflection symmetric scattering cases, i.e., when the co-pol and cross-pol are not close to zero. At this moment, an asymmetric volumetric scattering covariance matrix is used to an appropriate choice among the symmetric or asymmetric covariance matrices to find the best fit with model data (Yamaguchi et al. 2005). The result is a strong power of the volumetric scattering contribution (*Pv*), even in naturally non-distributed cloud dipoles as a forest environment.

Table 2 shows the results of the best models by the Δ AIC < 2 criteria, and the model-averaged importance of the polarimetric attributes. Eleven models were pre-selected by the Δ AIC < 2 criteria. Four polarimetric attributes occurred in 80% of the selected models. They were the ratio between HH and VV channels (*Rpp*), the terms imaginary and real off-diagonal of the coherency matrix **[T]**, and the volume power of the Bhattacharya decomposition.

The selected model with six parameters (1) was able to explain 65% of AGB variability of SFsat Manaus study site ($R^2adj.$ = 0.65; *RMSE* = 35.93 Mg ha^{-1}); and did not show evidence of multicollinearity by VIF (Table 3). Considering that LogLik and AIC had similar results when evaluating Akaike weights w_i, the first model presents a performance 30% higher than the second and 50% higher than the third (Table 2). The

off-diagonal terms of the **[T]** and **[C]** matrices have rarely been selected for retrieving forest AGB, due to the reflection asymmetry assumption. However, the importance of some polarimetric attributes argues against this assumption. For instance, the relative importance of Touzi component, which is formulated by the Kennaugh–Huynen scattering matrix of the coherent target scattering, i.e., distributed targets (Touzi, 2004). Also, the importance of four-component model-based on the Yamaguchi and Bhattacharya decompositions, which consider asymmetry target to describe model volumetric scattering better (Bhattacharya et al. 2015; Yamaguchi et al. 2005; Touzi, 2004).

The polarimetric attributes selected by MLR models in Table 3 have different levels of iteration with forest AGB. The parameter $T_{13}realC$ is the real part of the term T_{13} of coherence matrix **[T]** $T_{13}realC = 2\langle(S_{H.H.} + S_{V.V.})S_{H.V}^{*}\rangle$. We can infer that high AGB values presented higher T_{13} values or an increase of cross-talk between channels. The same occurs concerning the imaginary term $T_{12}imagC = \langle(S_{H.H.} - S_{V.V.})(S_{H.H.} + S_{V.V})^{*}\rangle$.

Shannon Entropy is the normalized contribution of the polarization degree of the matrix **[T]** (*SE_P_norm*), that means the random degree of two of electric fields targets, as two forest class, for instance (Réfrégier and Morio, 2006). So, the higher the value higher the standard degree of randomness, i.e., they are more depolarized with the AGB, which indicates that SE value increases with increasing AGB (Figure A.1). TVSM_phi_s1 is the Touzi target phase angle of the first eigenvector λ_1 and represents an unambiguous description of symmetric scattering phase. For asymmetric cases under the assumption of the roll-invariant decomposition of coherent target scattering, the Φs_1 solves the ambiguity of the scattering type phase in the electric field spherical-helices basis (Touzi, 2007); TVSM_phi_s1 is more out of phase with the increasing SFs AGB.

The increase of AGB seems to be more helical scattering-type and spatially heterogeneous. By using the Φs_1 parameter, Touzi (2007) observed clear discrimination between small shrubs and sedges in wetlands.

The cross-polarization Ratio (Rpc) is the ratio between HV and HH channel $\text{Rpc} = \sigma^0_{hv}/\sigma^0_{hh}$; values higher than one represent the largest volumetric contribution with surface scattering (Henderson and Lewis, 1998). The relative standard errors of the parameter's estimators were higher than Sy = 20%, except for the Bhattacharya volumetric scattering component (Sy = 11.5%, Table 3); all estimator parameters were significant at $\alpha = 0.05$ (Table 3).

The selected model shows well-distribution of the residuals regardless of the previous intensity use (Figure 7) and does not show evidence of heteroscedasticity (BP: 3.38, p-valor = 0.067). However, there is a tendency to overestimate low AGB values < 50 Mg ha^{-1} and underestimate AGB > 150 Mg ha^{-1} (Figure 8a), which is reflected in the positive and non-zero bias by the t-test: μbias = 1.3 Mg ha^{-1}, t = -2.21, p-value = 0.02 (Figure 8b). This behaviour is commonly reported in the literature due to the lack of SAR signal sensitive to the increase of forest AGB (Imhoff, 1995; Saatchi et al. 2011). Here, we also noticed an overestimation of low AGB values that may be due to high increment rates of SF AGB in the low-intensity use areas. Besides, there is a slight tendency to overestimate SF AGB submitted to previous low-intensity use (blue dots) and to underestimate SF AGB submitted to high-intensity use (green dots) (Figure 7 and Figure 8a). From these observations, we can infer that separated models by intensity class could be built in future research.

The error of prediction after the bootstrap cross-validation was low and represented 8.75% of the mean observed AGB (RMSEP = 8.8 ± 2.98 Mg ha^{-1}), as depicted in Figure 8a. The bias of the estimate was μbias = 1.3 ± 36.5 Mg ha^{-1} (Figure

8b). The RMSEP was low or at the same magnitude than the observed from other simple regression (Saatchi et al. 2011; Santos et al. 2016) and MLR model (Bispo et al. 2014).

Recent studies have focused on semi-empirical approaches based on the Water Cloud Model because these models seem to be insensitive to the increase of forest AGB, although the RMSE tends to increase in densely vegetated areas (Bharadwaj et al. 2015, Kumar et al. 2012).

3.2. Model Performance Considering Past Land Use

We tested the contribution of the previous land-use history over SF areas by including the period of active land-use (PALU) and clear-cut frequency (FC) in the MLR model. When running the "glmulti" variable selection criterion, seven models with AIC < 2 were generated, but only the first three presented all parameters with VIF < 10; therefore, the others were excluded from the analysis. Here we depicted only the selected model in Table 4.

As all models presented similar results, with at least one non-significant parameter at the level $\alpha = 0.05$, the second one was chosen because, besides presenting a smaller number of independent variables (6), it had VIF ≤ 2 of the parameters. This model was similar to the one obtained without the inclusion of PUS and FC variables in the model, except for the phase magnitude of the first Touzi component, which presented higher S.Y. % (Table 3).

The model with the inclusion of the land-use history was able to describe over 70% of AGB variability ($R^2adj. = 0.71$, $RMSEP = 8.2 \pm 2.63$ Mg ha^{-1}) of the secondary forests at Manaus study site. Besides, the AIC decreased from 1809.03 to 1781.24. Standardized residues presented behaviour similar to that observed for MLR without a

history of land-use (PALU and FC). The results suggested that the combination of backscattering power with multi-source data as land-use history, height index or interferometric coherence from InSAR (Bharadwaj et al. 2015; Kumar et al. 2012), local geomorphometric variables (Bispo et al. 2014), and polarimetric attributes would increase the accuracy of SFs AGB estimation across spatial scales and forest ages.

Finally, Figure 9 shows the SFs AGB in the study site. Note that young and early SF (aged 1 to 15 years) are preferentially located on both sides of BR-174, north of Manaus. Advanced S.F. stages (age > 16 years), on the other hand, are confused with primary forests because their boundaries are not distinguished from these.

3.3. Uncertainty report

The mean uncertainty was 7.5% ± 3.9% calculated by Eq (5). From the total uncertainty (Figure 10), the highest errors encompassed the plot expansion step, i.e., when forest biomass is scaled up from individuals to forest stands in hectare (26% Cassol et al. 2018a), followed by the reported land-use time-series (19% Carreiras et al. 2014), forest inventory (19%), and then regression model (15%). It is interesting to note that regression models (MLR) do not contribute to the highest errors in the AGB estimation. Errors from the field measurements, commonly known as ground truth, represent 53% of the total errors, which include, plot expansion, inventory measures, and allometry. Secondary forest Carbon sink on tropical forests remains with a high degree of uncertainty (Houghton et al. 2012; Aragão et al. 2014); except for studies at local scales (Neeff and Santos, 2005). Fast recovery of SF AGB associated with a high probability of re-clearance makes it challenging to estimate annual net carbon emissions in these areas. New platforms and sensors, as BIOMASS mission, which is designed with a P-band polarimetric sensor onboard, that can perform tomographic and repeat-pass

interferometry, set to be launched in 2022, would be appropriate to generate repeatedly SFs AGB across the tropics (Le Toan et al. 2011).

4. Conclusion

The selected MLR model with six parameters estimator was able to explain 65% of the biomass variability in secondary forest areas north of Manaus city, Central Amazonia. Prediction errors, obtained by cross-validation, were only 8.75% (8.8 Mg ha^{-1}). The main regression parameters of the MLR models involved unusual polarimetric decompositions and attributes as off-diagonal terms obtained from covariance **[C]** and coherence **[T]** matrices. The assumption of reflection symmetry may be relaxed on forest environments by the relative importance of its regression parameters. Considering past land-use history information, such as the frequency of clear cuts and the period of active land-use before abandonment on the input model, the model explains 71% of the SFs AGB. Relative uncertainty was 7.5 ± 3.8%, considering the different stages of the estimation procedures, from field measurements to SAR inversion models. Highest relative errors, however, were observed at the ground truth stages (inventory, allometry, and plot expansion), representing 53% of the total. These models can help us understand how the secondary forests interact with the different polarimetric attributes from the ALOS/PALSAR-2 data, and especially to increase the accuracy of biomass and carbon estimates in the study area, often covered by clouds.

Acknowledgement

Thanks for REGROWTH-BR, which provides images of land-use history, data of ALOS/PALSAR-2, and financial support for the field campaign. Thanks to JAXA to provide polarimetric images in the study site. We thank the field team, Richard Lucas, Egidio Arai, Virgílio Pereira, Josh Jones, Joana Mello, João M. de B. Carreiras,

Movido, and Caroço (parataxonomists).

Disclosure statement

The authors reported no potential conflict of interest

References

Ainsworth, T.L., J.S. Lee, and D.L. Schuler. 2000. "Multi-Frequency Polarimetric SAR Data Analysis of Ocean Surface Features." In *IGARSS 2000. IEEE 2000 International Geoscience and Remote Sensing Symposium. Taking the Pulse of the Planet: The Role of Remote Sensing in Managing the Environment. Proceedings (Cat. No.00CH37120)*, 3:1113–1115. Honolulu, HI, USA: IEEE. doi:10.1109/IGARSS.2000.858039.

Allain, S., L. Ferro-Famil, and E. Pottier. 2005. "New Eigenvalue-Based Parameters for Natural Media Characterization." In *European Radar Conference, 2005. EURAD 2005.*, 2005:197–200. IEEE. doi:10.1109/EURAD.2005.1605594.

Aragão, Luiz E O C, Benjamin Poulter, Jos B. Barlow, Liana O. Anderson, Yadvinder Malhi, Sassan Saatchi, Oliver L. Phillips, and Emanuel Gloor. 2014. "Environmental Change and the Carbon Balance of Amazonian Forests." *Biological Reviews* 89 (4): 913–931. doi:10.1111/brv.12088.

Bharadwaj, Sai, P., Shashi Kumar, S.P.S. Kushwaha, and Wietske Bijker. 2015. "Polarimetric Scattering Model for Estimation of above Ground Biomass of Multilayer Vegetation Using ALOS-PALSAR Quad-Pol Data." *Physics and Chemistry of the Earth, Parts A/B/C* 83–84. Elsevier Ltd: 187–195. doi:10.1016/j.pce.2015.09.003.

Bhattacharya, Avik, Arnab Muhuri, Shaunak De, Surendar Manickam, and Alejandro C. Frery. 2015. "Modifying the Yamaguchi Four-Component Decomposition Scattering Powers Using a Stochastic Distance." *IEEE Journal of Selected Topics in Applied Earth Observations and Remote Sensing* 8 (7): 3497–3506. doi:10.1109/JSTARS.2015.2420683.

Bispo, P. C., J. R. Santos, M. M. Valeriano, R. Touzi, and F. M. Seifert. 2014. "Integration of Polarimetric PALSAR Attributes and Local Geomorphometric Variables Derived from SRTM for Forest Biomass Modeling in Central Amazonia." *Canadian Journal of Remote Sensing* 40 (1): 26–42. doi:10.1080/07038992.2014.913477.

Brown, Sandra, Andrew J.R. Gillespie, and Ariel E Lugo. 1989. "Biomass Estimation Methods for Tropical Forests with Applications to Forest Inventory Data." *Forest Science*. http://www.ingentaconnect.com/content/saf/fs/1989/00000035/00000004/art00003.

Burnham, K.P., and D.R. Anderson. 2002. *Model Selection and Multimodel Inference: A Practical Information-Theoretic Approach (2nd Ed)*. *Ecological Modelling*. 2nd ed. New York, NY: Springer-Verlag. doi:10.1016/j.ecolmodel.2003.11.004.

Calcagno, Vincent, and Claire de Mazancourt. 2010. "Glmulti : An R Package for Easy Automated Model Selection with (Generalized) Linear Models." *Journal of Statistical Software* 34 (12): 29. doi:10.18637/jss.v034.i12.

Carreiras, João M B, Joshua Jones, Richard M. Lucas, and Cristina Gabriel. 2014. "Land Use and Land Cover Change Dynamics across the Brazilian Amazon: Insights from Extensive Time-Series Analysis of Remote Sensing Data." Edited by Bruno Hérault. *PLoS ONE* 9 (8): e104144. doi:10.1371/journal.pone.0104144.

Cassol, Henrique Luis Godinho, Shimabukuro, Yosio Edemir, Carreiras, João Manuel de Brito, and Moraes, Elisabete Caria. 2018. "Improved Tree Height Estimation of Secondary Forests in the Brazilian Amazon." *Acta Amazonica* 48 (3): 179–190. doi:10.1590/1809-4392201700844.

Cassol, Henrique Luis Godinho, João Manuel de Brito Carreiras, Elisabete Caria Moraes, Luiz Eduardo Oliveira e Cruz de Aragão, Camila Valéria de Jesus Silva, Shaun Quegan, and Yosio Edemir Shimabukuro. 2018. "Retrieving Secondary Forest Aboveground Biomass from Polarimetric ALOS-2 PALSAR-2 Data in the Brazilian Amazon." *Remote Sensing* 11 (1): 59. doi:10.3390/rs11010059.

Chazdon, R.L. Second Growth: The Promise of Tropical Forest Regeneration in an Age of Deforestation (University of Chicago Press, Chicago, IL, 2014), 485 pp.

Chazdon, R. L., E. N. Broadbent, D. M. A. Rozendaal, F. Bongers, A. M. A. Zambrano, T. M. Aide, P. Balvanera, et al. 2016. "Carbon Sequestration Potential of Second-Growth Forest Regeneration in the Latin American Tropics." *Science Advances* 2 (5): e1501639–e1501639. doi:10.1126/sciadv.1501639.

Cloude, S.R. 1985. "Target Decomposition Theorems in Radar Scattering." *Electronics Letters* 21 (1): 22–24. doi:10.1049/el:19850018.

Cloude, Sr, and E Pottier. 1997. "An Entropy Based Classification Scheme for Land Applications of Polarimetric SAR." *IEEE Transactions on Geoscience and Remote Sensing* 35 (1): 68–78. doi:10.1109/36.551935.

Durden, S.L., J.J. van Zyl, and H.A. Zebker. 1990. "The Unpolarized Component in Polarimetric Radar Observations of Forested Areas." *IEEE Transactions on Geoscience and Remote Sensing* 28 (2): 268–271. doi:10.1109/36.46706.

Feldpausch, Ted R, Susan J Riha, Erick C M Fernandes, and Elisa Vieira Wandelli. 2005. "Development of Forest Structure and Leaf Area in Secondary Forests Regenerating on Abandoned Pastures in Central Amazônia." *Earth Interactions* 9 (6): 1–22. doi:10.1175/EI140.1.

Freeman, Anthony, and S.L. Durden. 1998. "A Three-Component Scattering Model for Polarimetric SAR Data." *IEEE Transactions on Geoscience and Remote Sensing* 36 (3): 963–973. doi:10.1109/36.673687.

Gehring, Christoph, Manfred Denich, and Paul L. G. Vlek. 2005. "Resilience of Secondary Forest Regrowth after Slash-and-Burn Agriculture in Central Amazonia." *Journal of Tropical Ecology* 21 (05): 519–527. doi:10.1017/S0266467405002543.

Hall, Mark. 1999. "Correlation-Based Feature Selection for Machine Learning." University ofWaikato. doi:10.1.1.149.3848.

Henderson, F. Lewis,A. Principles and Applications of Imaging Radar: Manual of Remote Sensing, 3ed. vol. 2. New York:Wiley, 1998.

Holm, W.A., and R.M. Barnes. 1988. "On Radar Polarization Mixed Target State Decomposition Techniques." In *Proceedings of the 1988 IEEE National Radar Conference*, 249–254. IEEE. doi:10.1109/NRC.1988.10967.

Houghton, R. A., J. I. House, J. Pongratz, G. R. van der Werf, R. S. DeFries, M. C. Hansen, C. Le Quéré, and N. Ramankutty. 2012. "Carbon Emissions from Land Use and Land-Cover Change." *Biogeosciences* 9 (12): 5125–5142. doi:10.5194/bg-9-5125-2012.

Huynen, J. Richard. 1970. "Phenomenological Theory of Radar Targets."

Imhoff, M.L. 1995. "Radar Backscatter and Biomass Saturation: Ramifications for Global Biomass Inventory." *IEEE Transactions on Geoscience and Remote Sensing* 33 (2): 511–518. doi:10.1109/36.377953.

Kumar, Shashi, Uttara Pandey, Satya P. Kushwaha, Rajat S. Chatterjee, and Wietske Bijker. 2012. "Aboveground Biomass Estimation of Tropical Forest from Envisat Advanced Synthetic Aperture Radar Data Using Modeling Approach." *Journal of Applied Remote Sensing* 6 (1): 063588. doi:10.1117/1.JRS.6.063588.

Laurance, William F., José L. C. Camargo, Philip M. Fearnside, Thomas E. Lovejoy, G. Bruce Williamson, Rita C. G. Mesquita, Christoph F. J. Meyer, Paulo E. D. Bobrowiec, and Susan G. W. Laurance. 2018. "An Amazonian Rainforest and Its Fragments as a Laboratory of Global Change." *Biological Reviews* 93 (1): 223–247. doi:10.1111/brv.12343.

Lee, Jong-Sen, and Eric Pottier. 2009. *Polarimetric Radar Imaging: From Basics to Applications*. New York, NY: CRC Press: Taylor $ Francis Group. doi:10.1201/9781420054989.fmatt.

Le Toan, T., S. Quegan, M.W.J. Davidson, H. Balzter, P. Paillou, K. Papathanassiou, S. Plummer, et al. 2011. "The BIOMASS Mission: Mapping Global Forest Biomass to Better Understand the Terrestrial Carbon Cycle." *Remote Sensing of Environment* 115 (11). Elsevier Inc.: 2850–2860. doi:10.1016/j.rse.2011.03.020.

Lima, Adriano José Nogueira, Liliane Marins Teixeira, Vilany Matilla Colares Carneiro, Joaquim dos Santos, and Niro Higuchi. 2007. "Análise Da Estrutura e Do Estoque de Fitomassa de Uma Floresta Secundária Da Região de Manaus AM, Dez Anos Após Corte Raso Seguido de Fogo." *Acta Amazonica* 37 (1): 49–53. doi:10.1590/S0044-59672007000100005.

Motulsky, H J, and A Christopoulos. 2003. *Fitting Models to Biological Data Using Linear and Nonlinear Regression. GraphPad Software, Inc., San Diego, CA*. San Diego: GraphPad Software, Inc. doi:10.1002/sim.2181.

Neeff, Till, and João Roberto dos Santos. 2005. "A Growth Model for Secondary Forest in Central Amazonia." *Forest Ecology and Management* 216 (1–3): 270–282. doi:10.1016/j.foreco.2005.05.039.

Neumann, Maxim, Laurent Ferro-Famil, and Eric Pottier. 2009. "A General Model-Based Polarimetric Decomposition Scheme for Vegetated Areas." *European Space Agency, (Special Publication) ESA SP* 668 SP (October).

Nguyen, Viet Tateishi, Luong, Ryutaro Hoan, Nguyen, Thanh , Sharma, Ram C., To, Tu Trong, and Le, Son Mai. 2016. "Estimation of Tropical Forest Structural Characteristics Using ALOS-2 SAR Data." *Advances in Remote Sensing* 05 (02): 131–144. doi:10.4236/ars.2016.52011.

Pinheiro, José C.;Bates, Douglas M.; 2000. *Mixed-Effects Models in S and S-PLUS*. Edited by Jeffrey Q. Chambers, W. Eddy, W. Härdle, S. Sheather, and L. Tierney. Statistics and Computing. New York: Springer-Verlag. doi:10.1007/b98882.

Pope, Kevin O., Jose M. Rey-Benayas, and Jack F. Paris. 1994. "Radar Remote Sensing of Forest and Wetland Ecosystems in the Central American Tropics." *Remote Sensing of Environment* 48 (2): 205–219. doi:10.1016/0034-4257(94)90142-2.

Prates-Clark, Cássia da Conceição, Richard M. Lucas, and João R. dos Santos. 2009. "Implications of Land-Use History for Forest Regeneration in the Brazilian Amazon." *Canadian Journal of Remote Sensing* 35 (6): 534–553. doi:10.5589/m10-004.

R Development Core Team. 2008. "R: A Language and Environment for Statistical Computing." Vienna, Austria: R Foundation for Statistical Computing. http://www.r-project.org.

Réfrégier, Philippe, and Jérôme Morio. 2006. "Shannon Entropy of Partially Polarized and Partially Coherent Light with Gaussian Fluctuations." *Journal of the Optical Society of America. A, Optics, Image Science, and Vision* 23 (12): 3036–3044. doi:117913 [pii].Romanski, R. Kotthoff, L. CRAN, Package 'FSelector'. 2014.

Saatchi, Sassan S., Miriam Marlier, Robin L. Chazdon, David B. Clark, and Ann E. Russell. 2011. "Impact of Spatial Variability of Tropical Forest Structure on Radar Estimation of Aboveground Biomass." *Remote Sensing of Environment* 115 (11). Elsevier Inc.: 2836–2849. doi:10.1016/j.rse.2010.07.015.

Saatchi, Sassan S, Dubayah R, Clark, D, Chazdon, Robin, Hollinger, D. "Estimation of forest biomass change from fusion of radar and lidar measurements." in SENGEF 2010 Seminário de Atualização em Sensoriamento Remoto e Sistemas de Informações Geográficas Aplicados à Engenharia Florestal. Proceedings, 2010. Curitiba, Brazil.

Santos, João Roberto dos, Igor S. Narvaes, Paulo M. L. Graçaa, and Fábio Guimarães Gonçalves. 2009. "Polarimetric Responses and Scattering Mechanisms of Tropical Forests in the Brazilian Amazon." In Advances in Geoscience and Remote Sensing, edited by Gary Jedlovec, 183–206. InTech. doi:10.5772/8340.

Santos, João R, Camila V d. J Silva, Lênio S Galvão, Robert Treuhaft, José C Mura, Soren Madsen, Fábio G Gonçalves, and Michael M Keller. 2014. "Determining Aboveground Biomass of the Forest Successional Chronosequence in a Test-Site of Brazilian Amazon through X- and L-Band Data Analysis." In *Proc. SPIE*, edited by Diofantos G. Hadjimitsis, Kyriacos Themistocleous, Silas Michaelides, and Giorgos Papadavid, 9229:92291E. doi:10.1117/12.2066031.

Scheffer, M., S. R. Carpenter, T. M. Lenton, J. Bascompte, W. Brock, V. Dakos, J. van de Koppel, et al. 2012. "Anticipating Critical Transitions." *Science* 338 (6105): 344–348. doi:10.1126/science.1225244.

Shimada, Masanobu, Osamu Isoguchi, Takeo Tadono, and Kazuo Isono. 2009. "PALSAR Radiometric and Geometric Calibration." *IEEE Transactions on Geoscience and Remote Sensing* 47 (12): 3915–3932. doi:10.1109/TGRS.2009.2023909.

Silva, Roseana Pereira. 2007. "Alometria, Estoque e Dinâmica Da Biomassa de Florestas Primárias e Secundárias Na Região de Manaus(AM)." INSTITUTO NACIONAL DE PESQUISAS DA AMAZÔNIA – INPA.

Singh, Gulab, Yoshio Yamaguchi, and Sang-Eun Park. 2013. "General Four-Component Scattering Power Decomposition With Unitary Transformation of Coherency Matrix." *IEEE Transactions on Geoscience and Remote Sensing* 51 (5): 3014–3022. doi:10.1109/TGRS.2012.2212446.

Sinha, S., C. Jeganathan, L. K. Sharma, and M. S. Nathawat. 2015. "A Review of Radar Remote Sensing for Biomass Estimation." *International Journal of Environmental Science and Technology* 12 (5): 1779–1792. doi:10.1007/s13762-015-0750-0.

Small, David, and Adrian Schubert. 2008. *Guide to ASAR Geocoding*. *Rsl-Asar-Gc-Ad*. Zurich, Switzerland. doi:RSL-ASAR-GC-AD.

Steininger, Marc K. 2000. "Secondary Forest Structure and Biomass Following Short and Extended Land-Use in Central and Southern Amazonia." *Journal of Tropical Ecology* 16 (5): 689–708. doi:10.1017/S0266467400001656.

Touzi, R. 2004. "Target Scattering Decomposition of One-Look and Multi-Look SAR Data Using a New Coherent Scattering Model: The TSVM." In *IEEE International IEEE International IEEE International Geoscience and Remote Sensing Symposium, 2004. IGARSS '04. Proceedings. 2004*, 4:2491–2494. IEEE. doi:10.1109/IGARSS.2004.1369800.

Touzi, Ridha. 2007. "Target Scattering Decomposition in Terms of Roll-Invariant Target Parameters." *IEEE Transactions on Geoscience and Remote Sensing* 45 (1): 73–84. doi:10.1109/TGRS.2006.886176.

Treuhaft, Robert, Yang Lei, Fabio Gonçalves, Michael Keller, João Santos, Maxim Neumann, and André Almeida. 2017. "Tropical-Forest Structure and Biomass Dynamics from TanDEM-X Radar Interferometry." *Forests* 8 (8): 277. doi:10.3390/f8080277.

van Der Sanden, J J. 1997. *Radar Remote Sensing To Support Tropical Forest Management*. *Tropenbos-Guyana Series 5*. Wageningen, The Netherlands (Wageningen Agricultural University): Ponsen & Looijen bv, Wageningen. http://www.tropenbos.org/publications/radar+remote+sensing+to+support+tropical+forest+management+-++tropenbos+guyana+series+5.

van Zyl, Jakob J. 1993. "Application of Cloude's Target Decomposition Theorem to Polarimetric Imaging Radar Data." In *SPIE Conference on Radar Polarimetry*, edited by Harold Mott and Wolfgang-Martin Boerner, 1748:184. San Diego '92, 1992, San Diego, CA, United States. doi:10.1117/12.140615.

Wandelli, Elisa Vieira, and Philip Martin Fearnside. 2015. "Secondary Vegetation in Central Amazonia: Land-Use History Effects on Aboveground Biomass." *Forest Ecology and Management* 347 (July). Elsevier B.V.: 140–148. doi:10.1016/j.foreco.2015.03.020.

Woodhouse, I. Introduction to Microwave Remote Sensing. Boca Raton, FL: CRC Press, 2006.

Yamaguchi, Y., T. Moriyama, M. Ishido, and H. Yamada. 2005. "Four-Component Scattering Model for Polarimetric SAR Image Decomposition." *IEEE Transactions*

on Geoscience and Remote Sensing 43 (8): 1699–1706. doi:10.1109/TGRS.2005.852084.

Zhang, Lamei, Bin Zou, Hongjun Cai, and Ye Zhang. 2008. "Multiple-Component Scattering Model for Polarimetric SAR Image Decomposition." *IEEE Geoscience and Remote Sensing Letters* 5 (4): 603–607. doi:10.1109/LGRS.2008.2000795.

Appendix

Table A.1. Polarimetric attributes. Note: $[\mathbf{C}]_{3x3}$ covariance 3x3 matrix, $[\mathbf{T}]_{3x3}$ coherency 3x3 matrix, $[\mathbf{S}]_{2x2}$ Sinclair 2x2 matrix. The complete nomenclature can be accessed in Cassol et al. (2018a).

Input Matrix	Nº att.	Polarimetric Attributes	Reference
$[\mathbf{C}]_{3x3}$	9	I_C11, I_C12imag, I_C12real, I_C13imag, I_C13real, I_C22, I_C23imag, I_C23real, I_C33	Woodhouse (2006)
$[\mathbf{C}]_{3x3}$	3	Freeman_Dbl, Freeman_Odd, Freeman_Vol	Freeman and Durden (1998)
$[\mathbf{C}]_{3x3}$	2	ρhh-vv, |ρhh-vv|	Woodhouse (2006)
$[\mathbf{C}]_{3x3}$	3	Neumann_mDelta, Neumann_phDelta, Neumann_tau	Neumann, Ferro-Famil, and Pottier (2009)
$[\mathbf{C}]_{3x3}$	3	VanZyl_Dbl, VanZyl_Odd, VanZyl_Vol	van Zyl (1993)
$[\mathbf{C}]_{3x3}$	4	Yamaguchi_Dbl, Yamaguchi_Hlx, Yamaguchi_Odd, Yamaguchi_Vol	Yamaguchi et al. (2005)
$[\mathbf{C}]_{3x3}$	4	Bhattacharya_Dbl, Bhattacharya_Hlx, Bhattacharya_Odd, Bhattacharya_Vol	Bhattacharya et al. (2015)
$[\mathbf{C}]_{3x3}$	5	MCSM_Dbl, MCSM_DblHlx, MCSM_Odd, MCSM_Vol, MCSM_Wire	Zhang et al. (2008)
$[\mathbf{C}]_{3x3}$	4	Singh_Dbl, Singh_Hlx, Singh_Odd, Singh_Vol	Singh et al. (2008)
$[\mathbf{S}]_{2x2}$ $[\mathbf{T}]_{4x4}$	16	TVSM_alpha_s, TVSM_alpha_s1, TVSM_alpha_s2, TVSM_alpha_s3, TVSM_phi_s, TVSM_phi_s1, TVSM_phi_s2, TVSM_phi_s3, TVSM_psi_s, TVSM_psi_s1, TVSM_psi_s2, TVSM_psi_s3, TVSM_tau_s, TVSM_tau_s1, TVSM_tau_s2, TVSM_tau_s3	Touzi (2004)
$[\mathbf{T}]_{3x3}$	9	T11, T12imag,T12real,T13imag,T13real,T22,T23imag,T23real,T33	Woodhouse (2006)
$[\mathbf{T}]_{3x3}$	15	A - anisotropy, H - entropy, α – alfa angle, β – beta angle, λ – lambda angle, γ – gamma angle, δ – delta angle, p1, p2, p3, H.A., H_A, λ1, Λ2, Λ3	Cloude e Pottier (1997)
$[\mathbf{T}]_{3x3}$	9	T11_H, T12imag_H,T12real_H,T13imag_H,T13real_H,T22_H, T23imag_H,T23real_H,T33_H	Huynen (1970)
$[\mathbf{T}]_{3x3}$	9	T11_C,T12imag_C,T12real_C,T13imag_C,T13real_C, T22_C,T23imag_C,T23real_C,T33_C	Cloude (1985)
$[\mathbf{T}]_{3x3}$	9	T11_B,T12imag_B,T12real_B,T13imag_B,T13real_B, T22_B,T23imag_B,T23real_B,T33_B	Barnes-Holm (1988)
$[\mathbf{T}]_{3x3}$	6	SE – Shannon Entropy, SE_norm, SE_I, SE_I_norm, SE_P, SE_P_norm	Réfrégier e Morio (2006)
$[\mathbf{T}]_{3x3}$	4	SERD, SERD_norm, DERD, DERD_norm	Allain, Ferro-Famil, and Pottier (2005)
$[\mathbf{T}]_{3x3}$	1	P.H. - pedestal height	Durden, van Zyl, and Zebker (1990)
$[\mathbf{T}]_{3x3}$	1	P.F. – Polarization Fraction	Ainsworth, Lee, and Schuler (2000)
$[\mathbf{T}]_{3x3}$	1	RVI – Radar Vegetation Index	van Zyl (1993)
$[\mathbf{C}]_{3x3}$	3	VSI – Volume Scattering index, BMI – Biomass Index, CSI – Canopy Structure Index	Pope, Rey-Benayas, and Paris (1994)
$[\mathbf{C}]_{3x3}$	1	RFDI – Radar Forest Degradation Index	Saatchi et al. (2010)
$[\mathbf{C}]_{3x3}$	1	span (Tp) – Total power	Woodhouse (2006)
$[\mathbf{C}]_{3x3}$	2	Rcp - Cross-polarization ratio, Rpp – parallel polarization Ratio	Henderson and Lewis (1998)

$[\mathbf{C}]_{3x3}$	1	Forest	Nguyen et al. (2016)

Table 1. Description statistic of the nonlinear mixed effects model of Chapman-Richards model using "nlme" package. MSE – mean square error.

Model:	AGB ~ θ_1 (1 – e (-0.1225 age)) $^{\theta 3}$				
IC = 1					
Parameters:	Est.	Std.	Error	T-value	P(>|t|)
θ_1	187.1	9.1	20.5	2.0E-16	***
θ_3	0.84	0.14	6.0	1.2E-07	***
				MSE	37.4
IC = 2					
Parameters:	Est.	Std.	Error	T-value	P(>|t|)
θ_1	217.6	22.1	9.8	4.69E-11	***
θ_3	2.46	0.65	3.8	0.000641	***
				MSE	59.5
Random effects:		List (θ_1 ~ 1, θ_3 ~ 1)			
Level:	I.C.		Structure:	Diagonal	MSE
Correlation:	θ_1		θ_1	θ_3	
θ_3	0.26		0.0011	0.56	4.7

Table 2. Model description of ΔAIC < 2 selected by the exhaustive "glmulti" package. w_i are the weights given by the relative likelihood amongst models (Burnham and Anderson, 2002).

N	MLR Model	Nº (p)	Log Lik	AIC	w_i
1	~1+TVSM_phi_s1+Bhattacharya_Vol+SE_P_norm+T12_imagC+T13_realC+Rco	6	-896.5	1809.0	0.122
2	~1+TVSM_phi_s1+Bhattacharya_Vol+SE_P_norm+SE_norm+T12_imagC+T13_realC+Rco	7	-895.8	1809.5	0.094
3	~1+I_C33+TVSM_phi_s1+Bhattacharya_Vol+SE_norm+T12_imagC+T13_realC+Rco	7	-896.2	1810.3	0.065
4	~1+TVSM_phi_s1+Yamaguchi_Vol+Bhattacharya_Vol+ES_P_norm+ES_norm+T12_imagC+T13_realC+Rpp	8	-895.2	1810.4	0.062
5	~1+Bhattacharya_Vol+ES_P_norm+ES_norm+T12_imagC+T13_realC+Rpp	6	-897.2	1810.4	0.062

Table 3. Statistics of the selected MLR model to estimate AGB of secondary forests at Manaus study site. Sy – standard error; Sy – relative standard error (%), VIF – variance inflation factor.

Polarimetric attribute	Estimate	Sy	Sy (%)	p-value	VIF
(Intercept) ~1	-60.64	20.6	-34.0	0.0037	
TVSMphi_s1	0.71	0.3	46.1	0.0314	4.06
Bhattacharya_Vol	272.76	31.2	11.5	< 0.0001	2.26
SE_P_norm	34.77	14.8	42.6	0.0202	2.41
T12_imagC	910.79	274.1	30.1	0.0011	4.14
T13_realC	733.02	237.4	32.4	0.0024	1.03
Rpc	58.31	23.3	40.0	0.0134	1.38

Table 4. Statistics of the selected MLR model to estimate AGB of secondary forests at Manaus study site. Sy – standard error; sy – relative standard error (%), VIF – variance inflation factor.

Polarimetric attribute	Estimator	Sy	Sy (%)	p-value	VIF
(Intercept) ~1	-27.05	20.2	74.7	0.181	
Bhattacharya_Vol	259.40	28.9	11.1	0.000	2
SE_P_norm	30.35	13.8	45.5	0.030	2
T12_imagC	412.11	131.1	31.8	0.002	1
T13_realC	592.22	220.9	37.3	0.008	1
Rpp	46.85	21.7	46.3	0.032	1
Bhattacharya_Vol	259.40	28.9	11.1	0.000	2
PALU	-11.27	1.9	16.9	0.000	1
FC	2.82	1.3	46.1	0.034	1

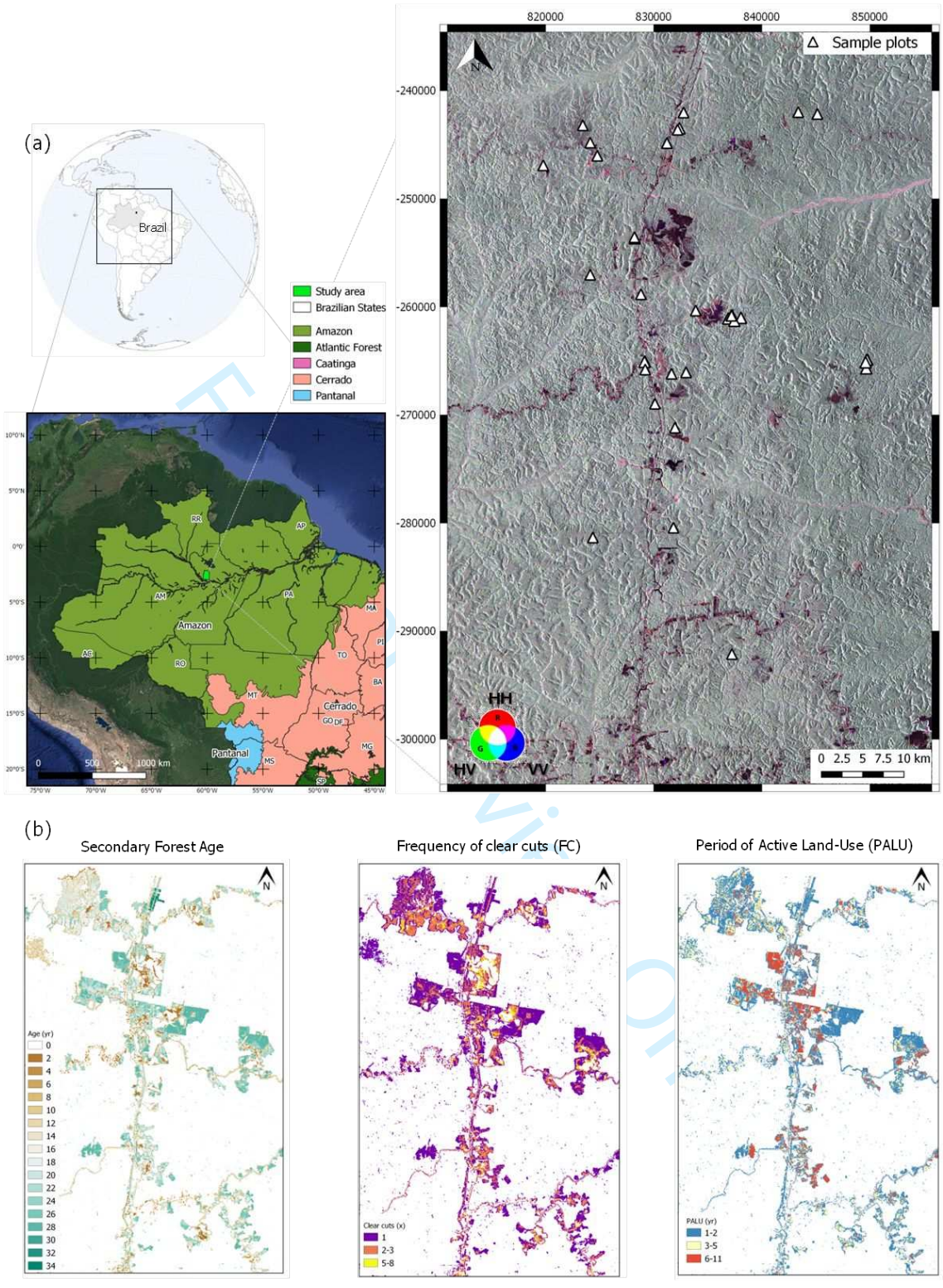

Figure 1. Location of the study area. (a) ALOS/PALSAR image in colour composition R(H.H.)G(H.V.)B(H.H.) highlighting inventory plot location (white triangle). (b) Classification of time-series of Landsat imagery to map several parameters of the secondary forests in the study site. Source: Carreiras et al. (2014).

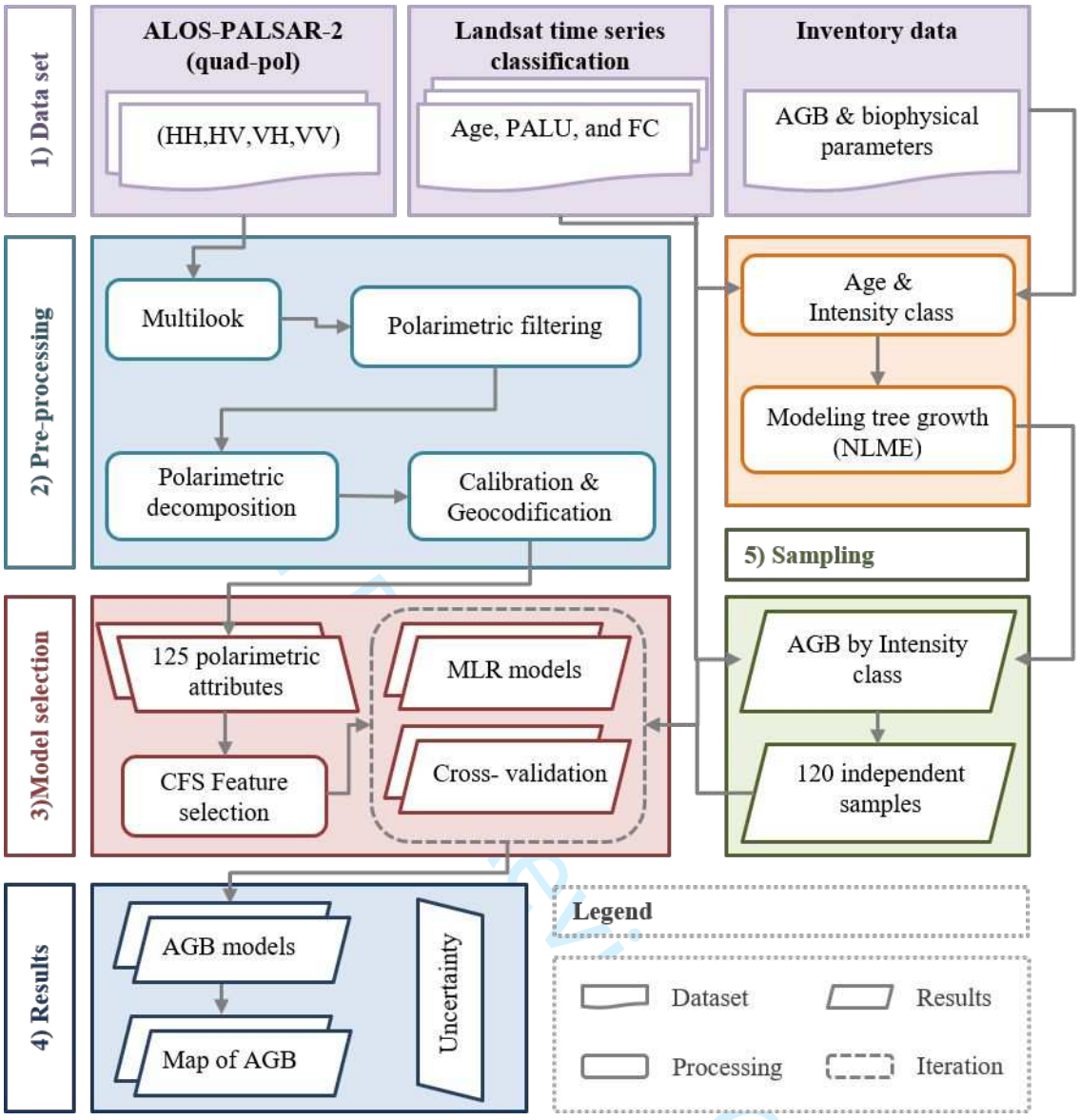

Figure 2. Methodological flowchart.

Figure 3. Profile of the secondary forests at Manaus study site regarding land-use before abandonment. A and B low-intensity class (IC = 1). C and D high-intensity class (IC = 2).

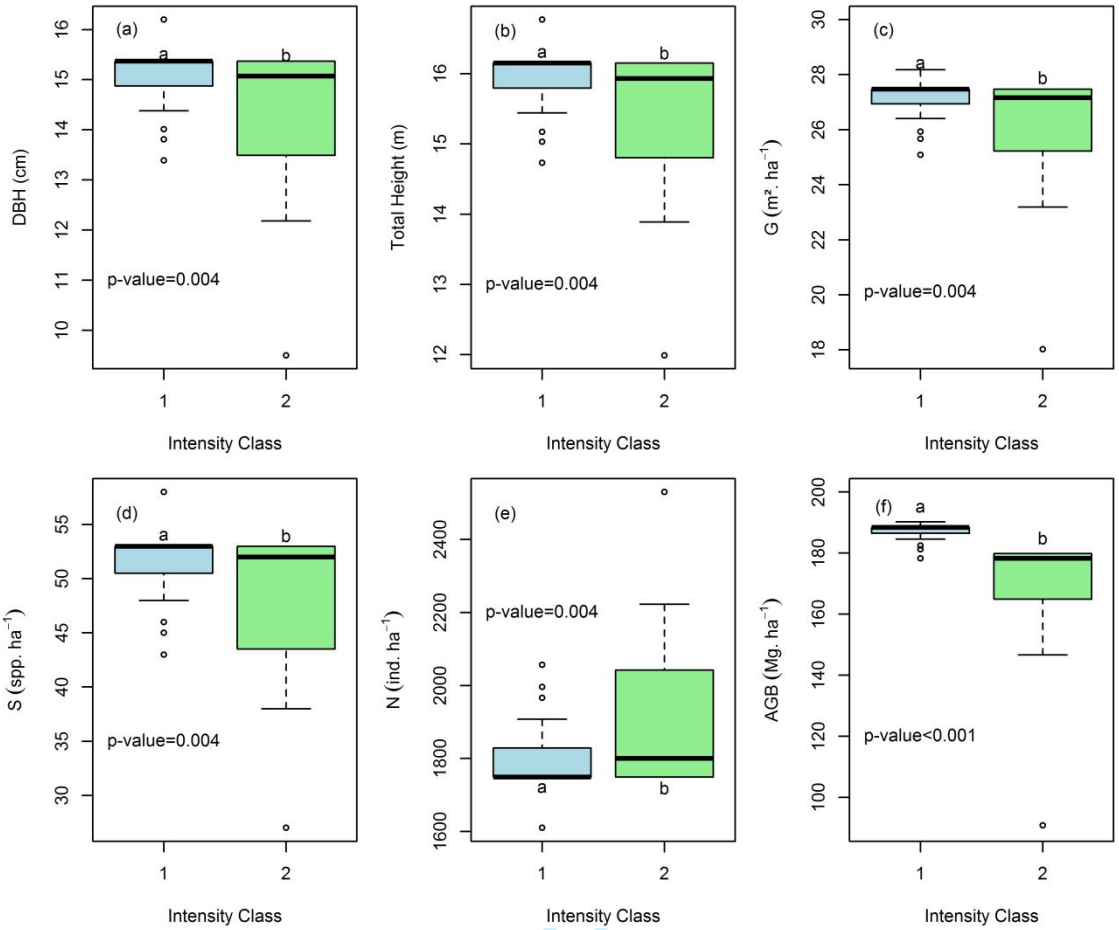

Figure 4. Distribution of phytosociological parameters by intensity class of previous use in secondary forests from Manaus: 1 – low-intensity; 2 – high-intensity. (a) Average diameter of breast height (DBH) at 1.3 m, DBH > 5cm (cm). (b) Mean tree height (m). (c) Basal area (G) (m^2 ha^{-1}). (d) Number of species per ha (S) (sp ha^{-1}). (e) Number of individuals DBH > 5 cm per ha (N) (ind ha^{-1}). (f) Above-ground biomass per ha (AGB) (Mg ha^{-1}).

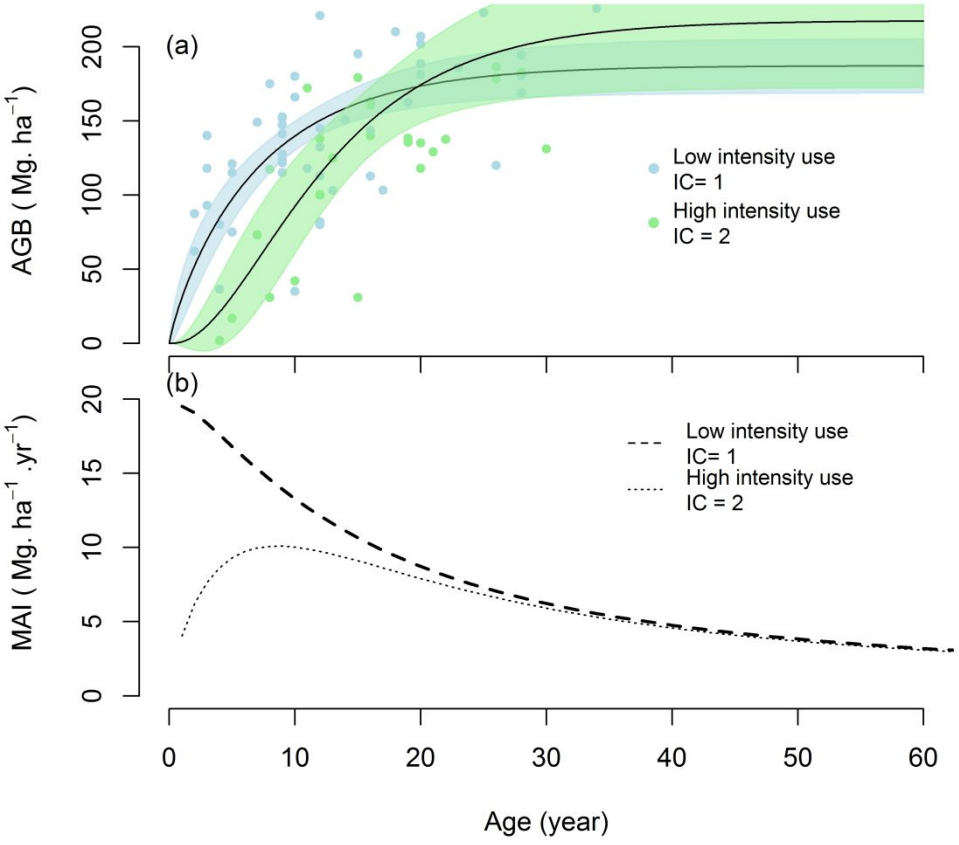

Figure 5. Growth curves of the secondary forest by intensity class. (a) Above-ground biomass accumulation by stand age, in years. Confidence intervals are represented in light shade areas. (b) Mean annual increment of AGB by age.

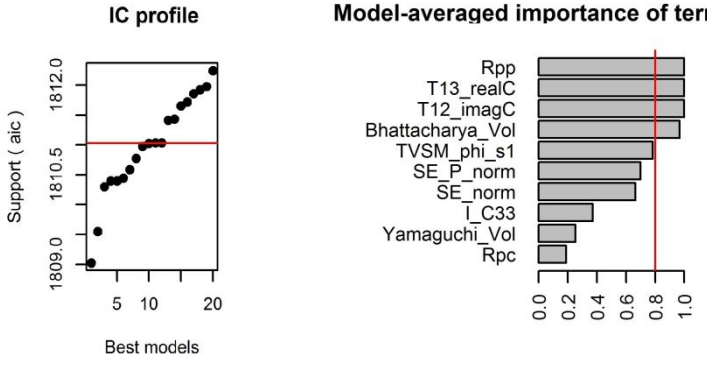

Figure 6. Performance of multiple linear models with CFS using "glmulti" exhaustive model selection algorithm. The x-axis in the right figure refers to partial importance correlation of each variable in the model.

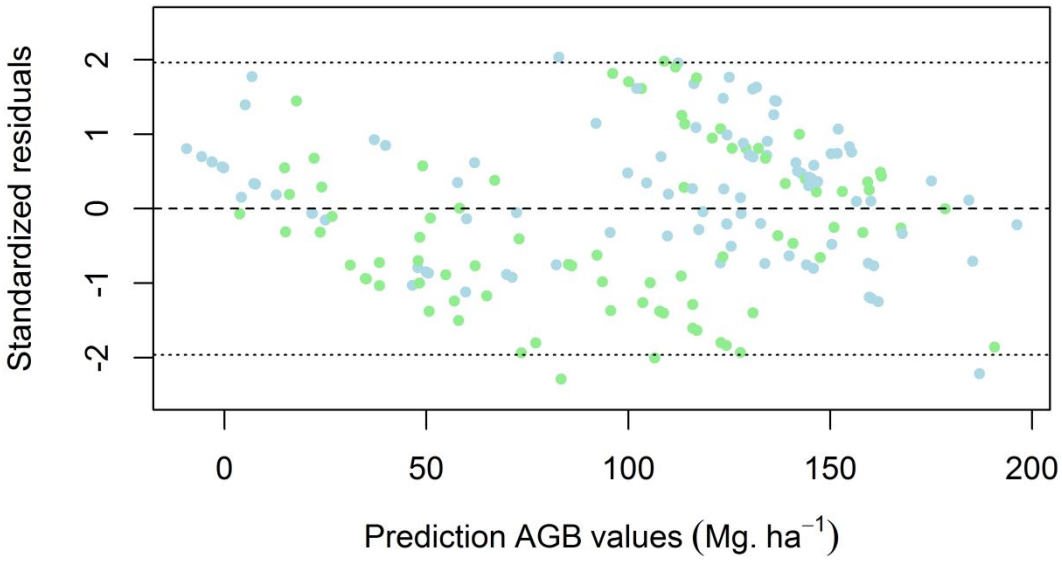

Figure 7. Distribution of standardized residues for the multiple linear model selected. Blue dots are low-intensity use plots, and green dots are high-intensity use areas. The dotted line is ± 1σ. The dashed line is the perfect residual fit.

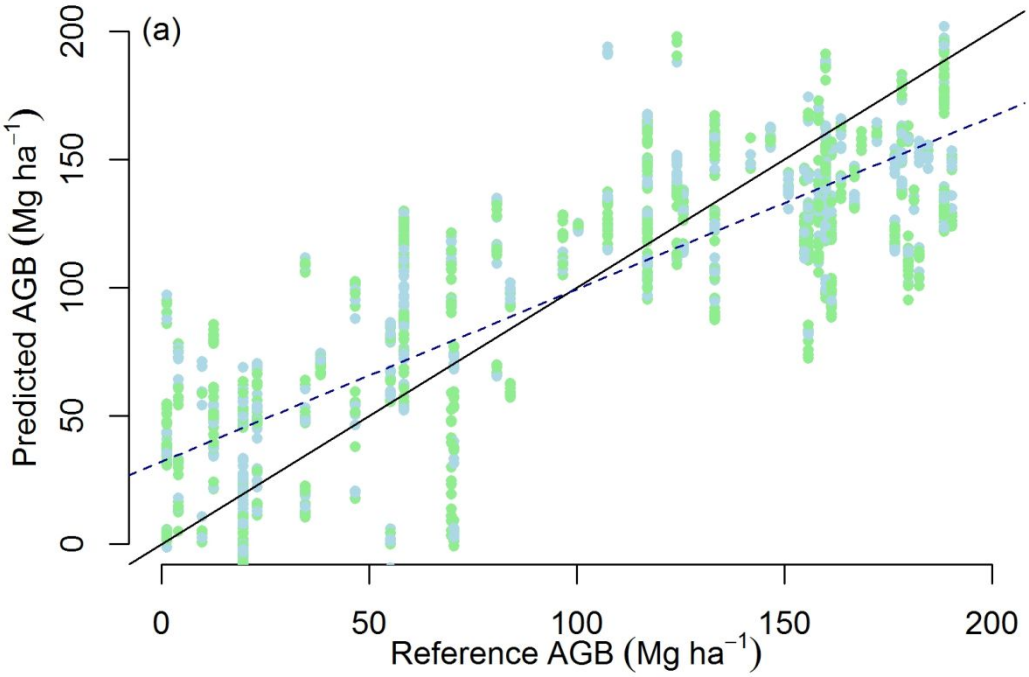

Figure 8. Cross-validation of MLR for AGB estimation at Manaus study site. A) Biomass distribution after bootstrapping cross-validation between the estimated and observed AGB values. The solid line represents the perfect 1:1 fit and the dotted line the adjustment after cross-validation $R^2 = 0.65$; RMSEP = 8.8 ± 2.98 Mg ha^{-1}. B) Probability density histogram of AGB bias after bootstrapping. Blue bars are low-intensity use plots, and green bars are high-intensity use areas.

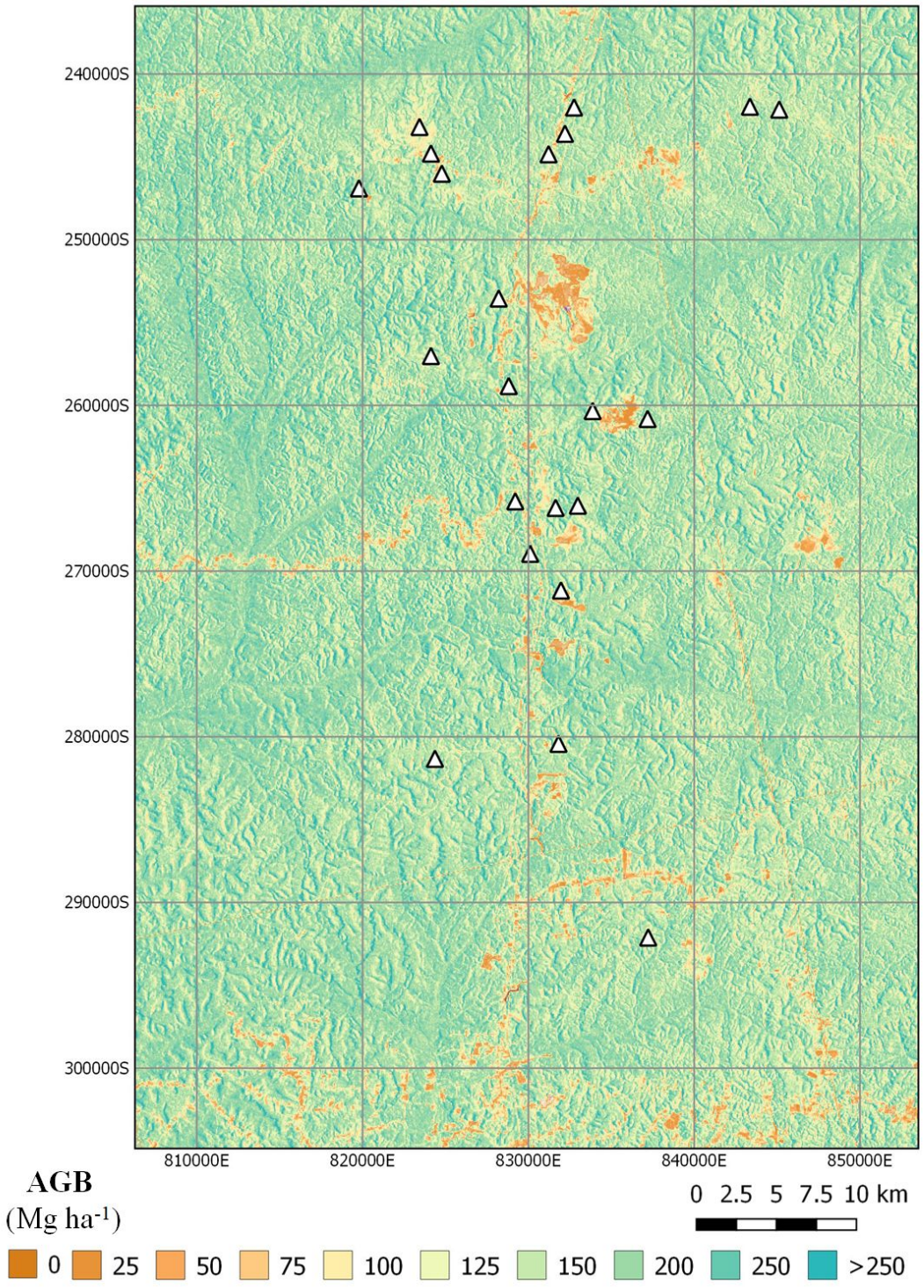

Figure 9. Above-ground biomass map in the study site.

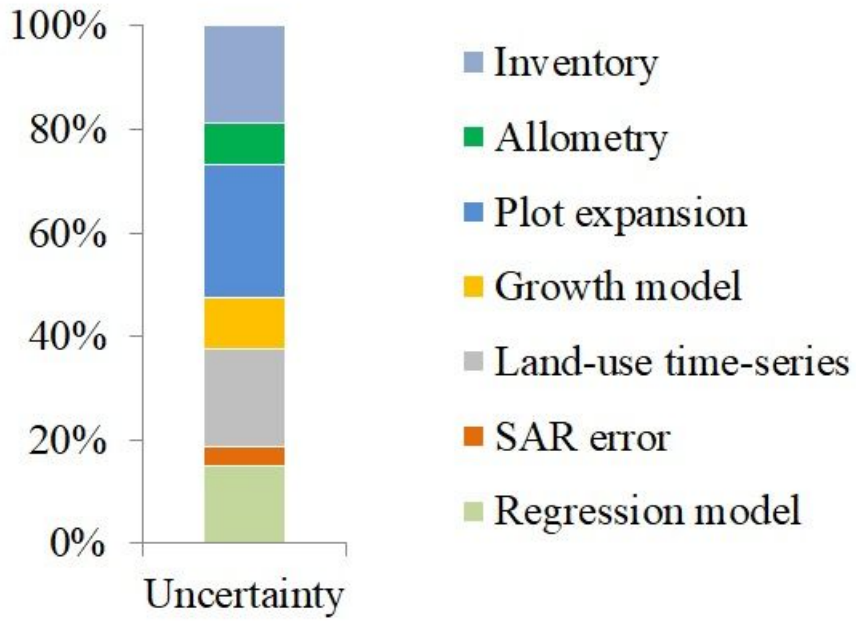

Figure 10. Partial uncertainty assessment in different stages for retrieving SFsbiomass with SAR data.

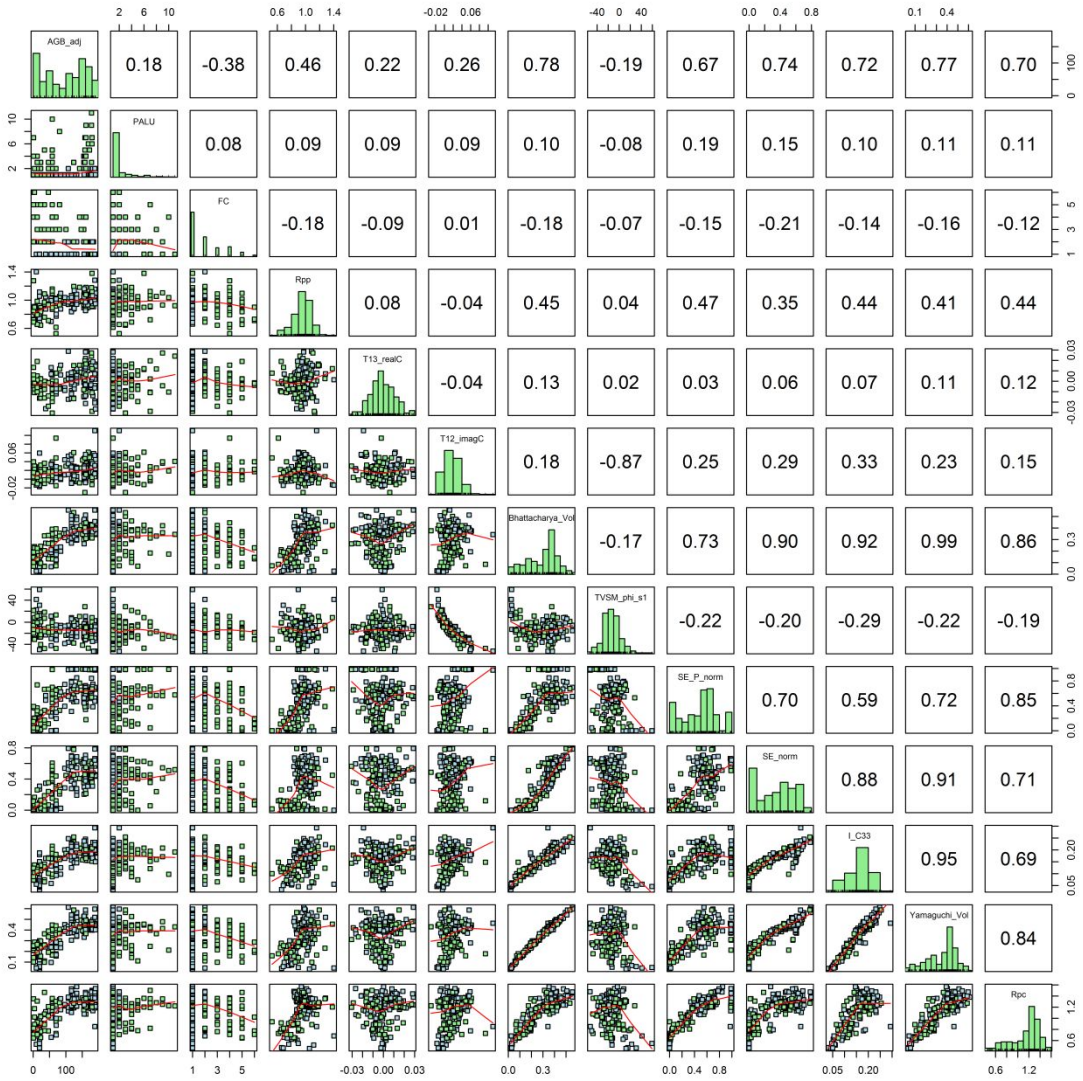

Figure A.1. Correlation matrix between AGB and the polarimetric attributes from CFS selector of the ALOS/ PALSAR-2. Note: AGB_adj – Above-ground biomass adjusted by growth curves; PALU – the period of active land-use; F.C. – frequency of clear cuts; Rpp – parallel polarization Ratio between V.V. and H.H. channel (1 > dominant double-bounce scattering, <1 dominant odd-bounce scattering) Rpp $= \sigma^0_{vv}/\sigma^0_{hh}$; T13_realC – real term off-diagonal of the coherency matrix $T_{13} = 2\langle(S_{H.H.} + S_{V.V.})S^*_{H.V.}\rangle$; T12_imagC – imaginary term off-diagonal of the coherency matrix $T_{12} = \langle(S_{H.H.} - S_{V.V.})(S_{H.H.} + S_{VV})^*\rangle$; Bhattacharya_Vol – volumetric contribution of Bhattacharya decomposition; TVSM_phi_s1– Touzi target phase angle of the first eigenvector (Φs_1); SE_P_norm and SE_P – contribution of the Shannon Entropy polarimetry normalized ([0, 1]; 0 = depolarized entropy, 1 = polarized entropy) SE_P

$= \log(1 - p_T{}^2)$, $p_T = \sqrt{1 - 27|[T]|/Tr[T]^3}$; I_C33 – third element of the covariance matrix $C_{22} = \langle |S_{V.V.}|^2 \rangle$. Yamaguchi_Vol – volumetric contribution of Yamaguchi decomposition; Rpc – cross-polarization Ratio is the ratio between H.V. and HH channel (1 > higher volumetric contribution in relation to surface scattering) $Rpc = \sigma^0_{hv}/\sigma^0_{hh}$.